Russian Geology and Geophysics © 2020, V.S. Sobolev IGM, Siberian Branch of the RAS
Vol. 61, No. 7, pp. 715–722, 2020 *DOI:10.15372/RGG2019074* *Geologiya i Geofizika*

Coseismic Motion on the Delta Fault within the Sherashevo–Inkino Site (Baikal Area): GPR Evidence

I.A. Denisenko[a, ✉], O.V. Lunina[a], A.S. Gladkov[a], A.V. Kazakov[b], E.V. Serebryakov[b], A.A. Gladkov[b]

[a] *Institute of the Earth's Crust, Siberian Branch of the Russian Academy of Sciences, ul. Lermontova 128, Irkutsk, 664033, Russia*

[b] *Irkutsk National Research Technological University, ul. Lermontova 83, Irkutsk, 664074, Russia*

Received 26 October 2018; received in revised form 23 January 2019; accepted 5 February 2019

Abstract–Ground Penetrating Radar (GPR) surveys in the area between Sherashevo and Inkino villages provide insights into the structure of the Delta Fault and allow estimating the amount of vertical slip caused by the $M = 7.5$ Tsagan earthquake of 12 January 1862. The surveys with shielded AB-90 and AB 250-M antennas of an *OKO-2* georadar along five profiles spaced at 25 m reveal normal slip from 2.6 to 4.5 m in different segments of the main seismogenic fault. The surface rupture caused by the 1862 event is traceable in interpreted radar images together with subsidiary faults; some possibly resulted from the 1959 Middle Baikal earthquake ($M = 6.8$). The GPR data are used to construct a 3D model of the area, which illustrates the evolution of the Delta Fault scarp since the Tsagan earthquake. Much of surface rupture during the Tsagan event is due to gravity sliding, judging by the amount of displacement estimated from GPR, structural, and field data of different years. Comprehensive understanding of the displacement pattern along the seismogenic fault requires further study extended to other segments of the fault zone.

Keywords: fault, Tsagan earthquake, GPR, coseismic motion, Lake Baikal

INTRODUCTION

The Delta Fault responsible for the disastrous Tsagan earthquake of 1862 on the eastern shore of Lake Baikal runs in the NE direction along the Tvorogovo Village – Kudara Valley – Oblom Cape, at an average NW dip of 60° (Fig. 1). It comprises several seismogenic structures and has been the cause of many instrumental earthquakes at its ends. The Tsagan earthquake generated by the fault produced a series of closely spaced stepped normal faults in Quaternary deposits (Lunina et al., 2009).

The Tsagan earthquake of the 12th January of 1862 was the largest on Lake Baikal for the historic time, with a magnitude of $M = 7.5$ and a shaking intensity of 10 (Solonenko and Treskov, 1960). The event was well documented at that time, since the first detailed report of January 1962 by N. Lopatin, a mining engineer, who visited the epicentral area. That is how Lopatin described rupture in soft sediments in his paper published in a local newspaper of Irkutsk (Amur, February 1862): "multiple wide-gaping fractures were opening along the slope of a sand-clay scarp and issued water flows; numerous other fractures were winding in different directions" (Lopatin, 1862).

Three years later, A. Fitingof (1865) published an article in Mining Journal where he reported about many fractures striking in the SW–NE direction and estimated the amount of tectonic subsidence as 4.26 m from the offset of a farm field fence between the villages of Dubinino and Oimur. According to Solonenko and Treskov (1960), the earthquake caused 7–8 m ground subsidence and produced the 200 km^2 Proval Gulf. Seismogeological trenching of the scarp toe in the early 1990s revealed round to conical planes of landslides, colluvial wedges, contortion, deformed beds, and a dense fracture network (Del'yansky, 1993; Khromovskikh, 1995).

Secondary coseismic deformation studied in the epicentral area of the Tsagan event (Lunina et al., 2012) occurred under NW–SE extension and formed a system of stepped normal faults striking mainly to 300–350° and dipping at angles of 45–75°, with a vertical offset of 2.83 m, as measured in a reference layer in a trench.

The amount of slip measured in different parts of the Delta Fault ranges from the greatest value of 8 m estimated from the lake depth at the Oblom Cape (Kondorskaya and Shebalin, 1982) to 2.8 or 4.26 m according to other estimates elsewhere along the fault. Thus varying offsets are generally common to seismogenic faults (Strom and Nikonov, 1997; McCalpin, 2009).

Currently, geological structures are often studied by ground penetrating radar (GPR) surveys. The method is ad-

✉ Corresponding author.
E-mail address: denisenkoivan.1994@mail.ru (I.A. Denisenko)

vantageous over other methods of shallow geophysics in high resolution, performance, and quick quality check. It has imaged the fault structure to quite a good resolution till a depth of 20 m, which hardly can be done by the conventional techniques. GPR is used broadly worldwide to study active faults (Salvi et al., 2003; Robert et al., 2010; Fischer et al., 2012; Yalciner et al., 2013; Brandes, 2018) but is still of limited use in Russia despite successful experience (Varenkov et al., 2006; Tarabanko, 2007; Lunina et al., 2016, 2018). This study aims at imaging the structure of the Delta Fault and estimating the slip caused by the Tsagan earthquake of 1862 between the villages of Sherashevo and Inkino. The results contribute to the understanding of deformation on normal fault planes in different parts of the seismogenic zone and allow modeling the 3D structure and geomorphology of the area at the time of the earthquake and at present.

METHODS

Faults within the damage zone of the Delta Fault were detected and traced within a specially selected test site between Sherashevo and Inkino villages (Fig. 1), by ground penetrating radar (GPR) surveys along five profiles (Figs. 1, 2) spaced at 25 m, with the lengths 130 m (profiles 1, 2, 3), 140 m (profile 4), and 160 m (profile 5).

GPR is a high-resolution geophysical method based on the propagation of high-frequency electromagnetic waves and receiving reflections from dielectric interfaces (Vladov and Starovoitov, 2004). The GPR surveys were performed by an *OKO-2* radar with AB-90 (central frequency 90 MHz) and AB 250M (250 MHz) shielded antennas, which can reach depths of 18 m and 8 m and provide resolutions of 0.5 m and 0.25 m, respectively.

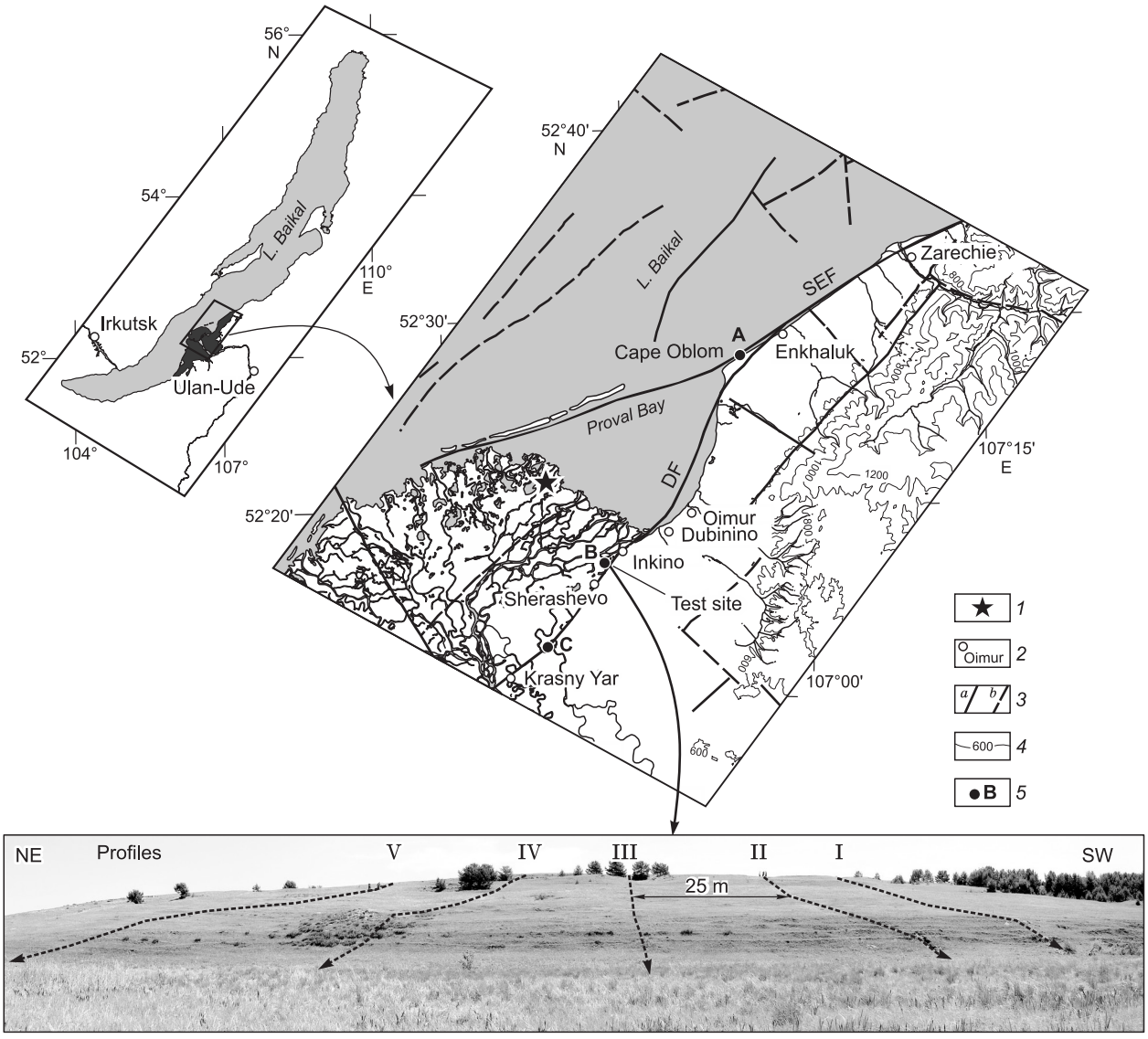

Fig. 1. Location map of study area. *1*, earthquake epicentral area, after (Lunina et al., 2012); *2,* villages; *3*, observed (a) and inferred (b) faults, after (Lunina et al., 2012); *4*, contour lines (at 200 m); *5*, sites for fault offset measurements. Abbreviations stand for: DF, Delta Fault; SEF, Sakhalin–Enkhaluk Fault.

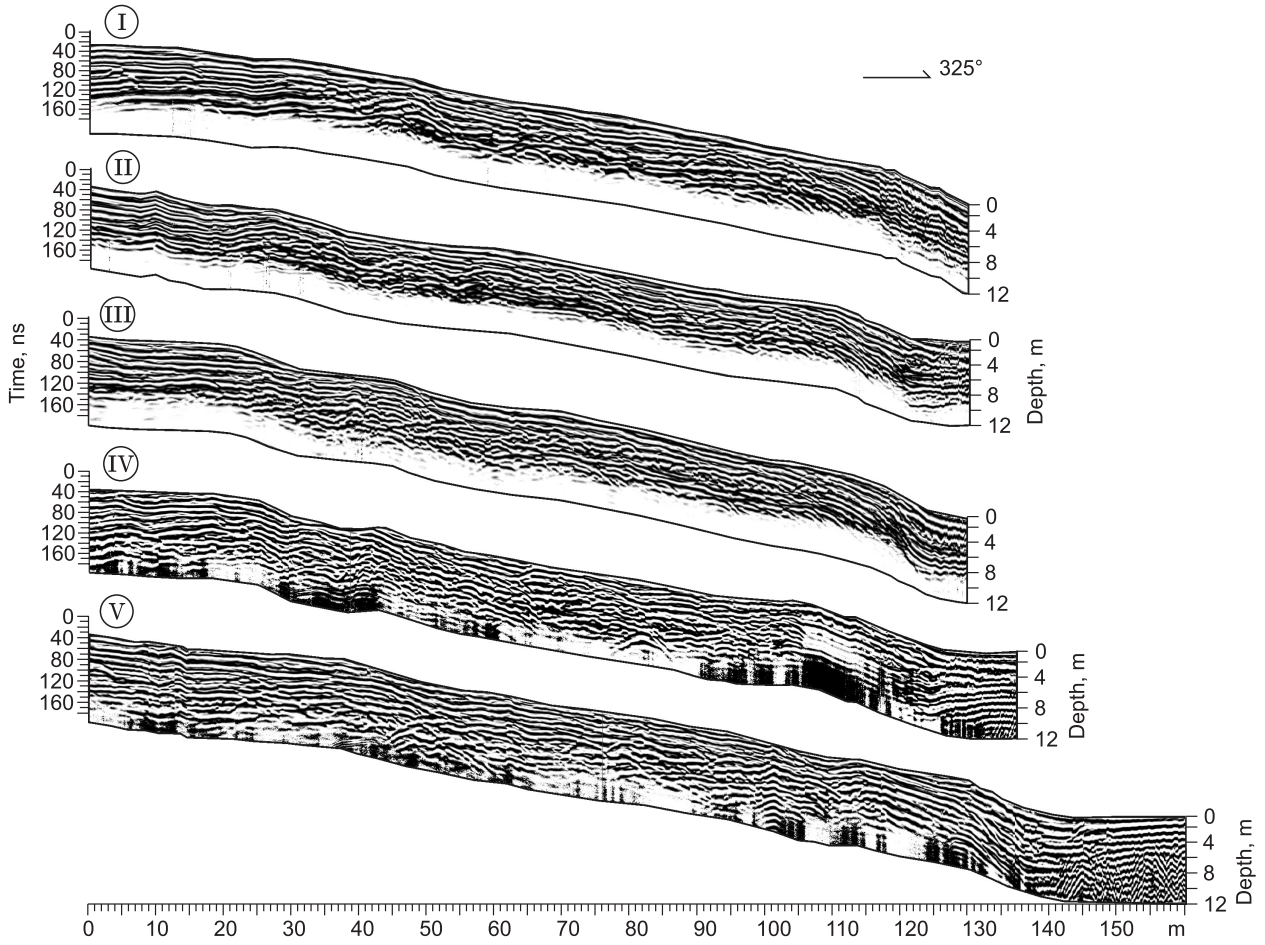

Fig. 2. Preprocessed radar images along profiles 1–5.

The data were interpreted with regard to elevations measured by a Leica Geosystems total station at every 1.0–1.5 m. Geological boundaries were determined by drilling and coring to a maximum depth of 15 m (Fig. 3) using a UKB 12/25 auger rig. The drilling results revealed a homogeneous section composed of silt, fine or very fine sand, and clay silt throughout the area. The GPR data were processed in GeoScan32, in several steps. First, dielectric permittivity of the ground, as a penetration control, was estimated as $\varepsilon = 5.1$, from noise features in radar images (unwanted inclined linear reflections or diffraction hyperbolas), with reference to core data. The following steps included choice of time gain, brightness, and contrast, analysis of noise for updating the dielectric parameters of rocks, and elevation correction. The signal-to-noise ratio was improved by the conventional techniques of running average, low pass or bandpass filtering, and background trend subtraction (Vladov and Starovoitov, 2004). At the final step, the radar wave patterns were matched to the sedimentary layers stripped in boreholes. The layer boundaries in the wave pattern followed reflection events. Main faults within the Delta Fault zone were detected proceeding from changes in the GPR wave patterns (offsets and/or abrupt attenuation).

RESULTS

According to the GPR processing, large faults are located mainly within the scarp of the seismogenic Delta Fault, with its top surface, slope, and floor dipping, respectively, at 2–11°, 23–40°, and 0–2°. The dip of the main fault plane detected by GPR data varies from 60 to 80°. The interpretation focused on the fragments of GPR images corresponding to the scarp.

The GPR data along profile I reveal five units composed of light brown fine to medium sand that encloses scarce lumpy humus and plant rootlets (Unit 1); fine sand with clay silt lenses (Unit 2);

And massive light brown fine silty sand with scattered small mottles of limonitized sand (Unit 3). Units 4 and 5, lying beyond the reach depth of the boreholes, were distinguished from the geophysical surveys only. The wave pattern within the 119–127 m interval of profile distances shows signatures of two quasi-parallel steep (75° and 81°) ruptures spaced at 5 m. The top of Unit 2 is offset 2.6 m along one of them, while the offset of the base is obscured by noise of unknown origin between 116 and 119 m (Fig. 4, I).

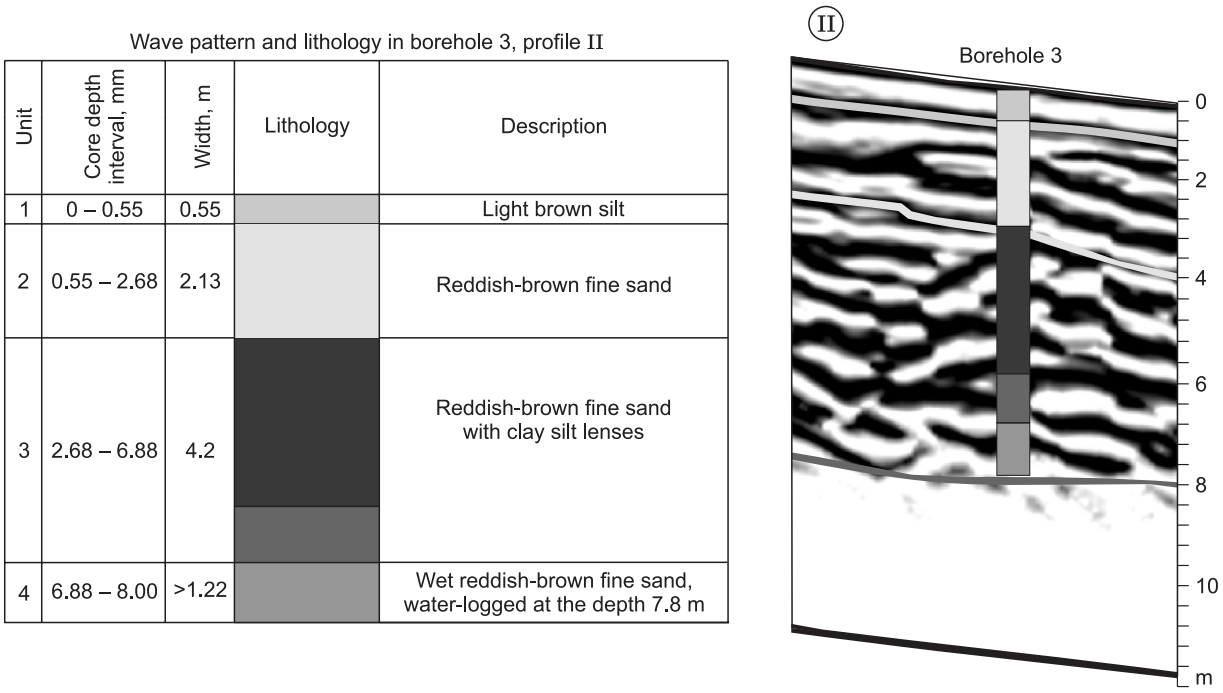

Fig. 3. Fragment of radar image with wave pattern and lithology in borehole 3.

The GPR data along profile II interpreted to more detail reveal a unit of peat-bearing sediments in addition to the above five units. The wave pattern in the 117–125 m distance interval records a large normal fault, with its plane dipping at 83° and a vertical offset of 3 m, delineated by an anomaly which may correspond to a zone of liquefied material (Fig. 4, II.).

Profile III is identical to profile II, likewise with six units and a normal fault plane dipping at 79°, with a vertical slip of 3.4 m (Fig. 4, III).

The GPR data along profile IV show five units, of which three were presumably shifted along the fault (Fig. 5). A large normal fault, with an offset of 4.5 m, surrounded by four subsidiary faults, appears in the 115–130 m interval. The data at distances 106 to 111 m are noisy: the profile crossed a concrete basement, which however did not cause any significant influence on the results.

The geological boundaries were observed more precisely in a trench dug specially during surveys along profile II, with its location selected after the preliminary interpretation of the GPR data at 2.4 m far from the concrete basement (Fig. 5). The trench was 2.94 m deep, 2.2 m long, and 0.6 m wide, and was oriented at an azimuth of 325°. It stripped a zone of deformation, with two parallel rupture planes dipping at 45°, 1.4 m apart, at a depth of 1.3 m (Fig. 5), along which sediments descended stepwise from northwest to southeast. The amount of displacement along the northwestern plane was 0.4 m. Both ruptures are detectable in the higher-frequency AB-250 image but merge into a single structure in that of AB-90.

The sediments within the 0.15–1.3 m depth range appearing in the trench walls and in the radar images belong to Unit 1, while the rocks below 2.94 m are lithologically homogeneous.

The data along GPR profile V reveal a different pattern. The profile follows a topographic slope of 22° shallowing down gradually from NE to SW. The wave pattern (Fig. 4, V) highlights a 16 m wide graben-like basin delineated by several synthetic and antithetic normal slip planes. The SE fault has a dip of 60° and a vertical offset of 4.4 m, while the NW one dips at 50° and has a smaller slip (1.4 m). The inner part of the graben is cut by small local ruptures with dips of 50–57° and a vertical slip of 0.7 m. The SE normal fault crosscuts an interface of unclear origin near the scarp crest at ~65°.

DISCUSSION

The GPR surveys within a 10 750 m^2 site show a heterogeneous structure of the fault zone axis, with isolated parallel ruptures in some segments and graben of a variable width in others. The surveys along profile I likely failed to see the

Table 1. Amounts of vertical offset in different segments of Delta Fault

Location (Fig. 1)	Vertical slip, m	Reference
Cape Oblom	8	Kondorskaya and Shebalin, 1982
Sherashovo – Krasny Yar	2.83	Lunina et al., 2012
Dubinino – Oimur	4.26	Fitingof, 1865
Inkino – Sherashovo	2.6 to 4.6	This study

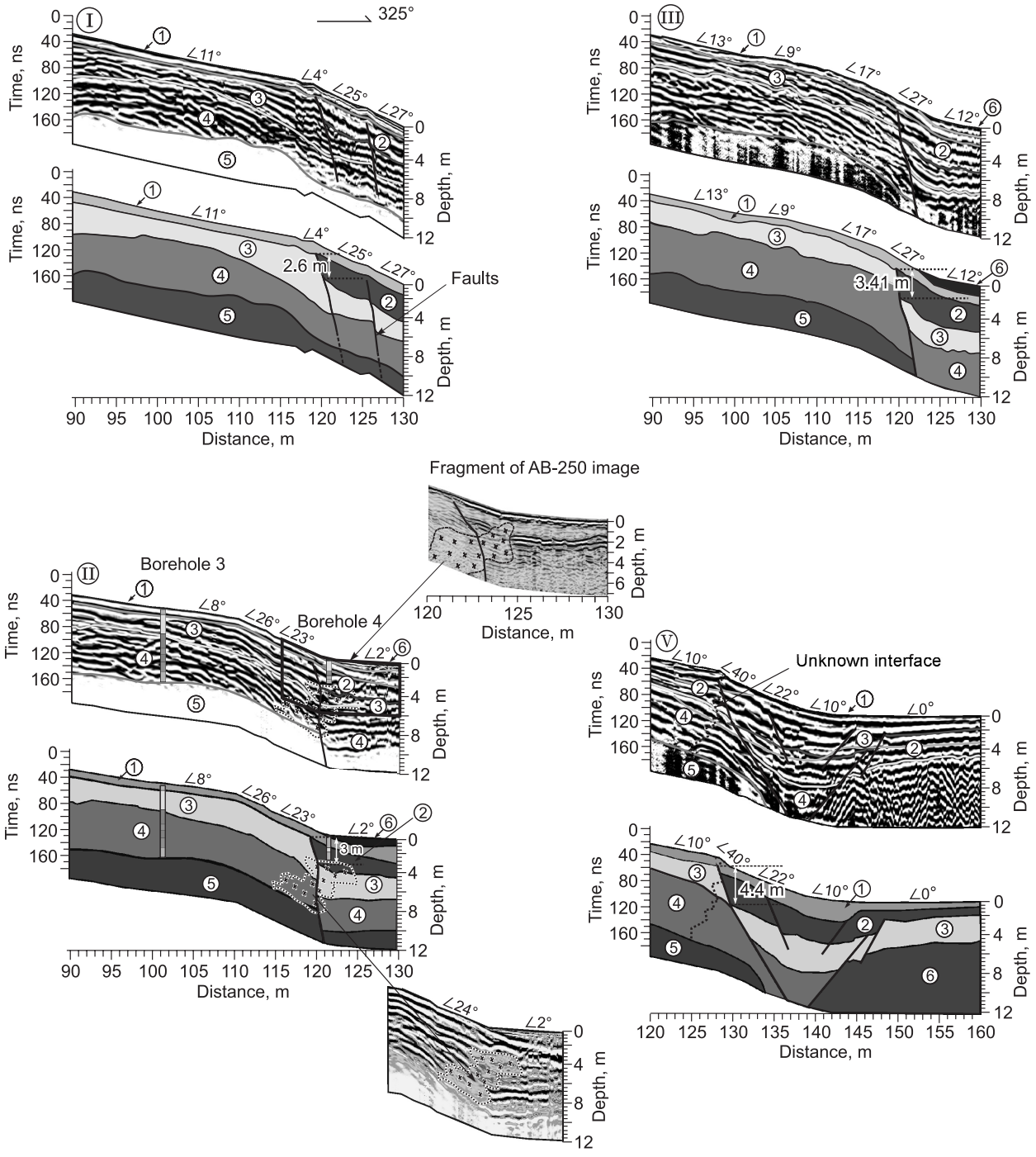

Fig. 4. Fragments of radar images across the Delta Fault and their interpretation (between Sherashevo and Inkino villages). Roman numerals are numbers of profiles; numerals in circles are numbers of units. Dash line in inset for profile II contours the zone of liquefied sediments.

conjugate normal fault. The amount of vertical slip increases from 2.6 to 4.5 m from SW to NE in different fault zone segments. This change over a 120 m long site traces regularly increasing slip on the seismogenic fault toward the earthquake epicenter which was located from the distribution of coseismic deformation structures (Lunina et al., 2012).

The largest 8 m coseismic vertical slip on the Delta Fault during the Tsagan earthquake (Kondorskaya and Shebalin, 1982) differs markedly from those in other segments estimated by different methods (Fitingof, 1865; Lunina et al., 2012; this study). The 8 m slip was inferred from the lake depth in the Proval Gulf and may have been overestimated because the block that formerly corresponded to the Tsagan Steppe likely slid by gravity. The gravity sliding hypothesis agrees with the fact that the offset is the largest at the end of the rupture rather than in its central part as it commonly oc-

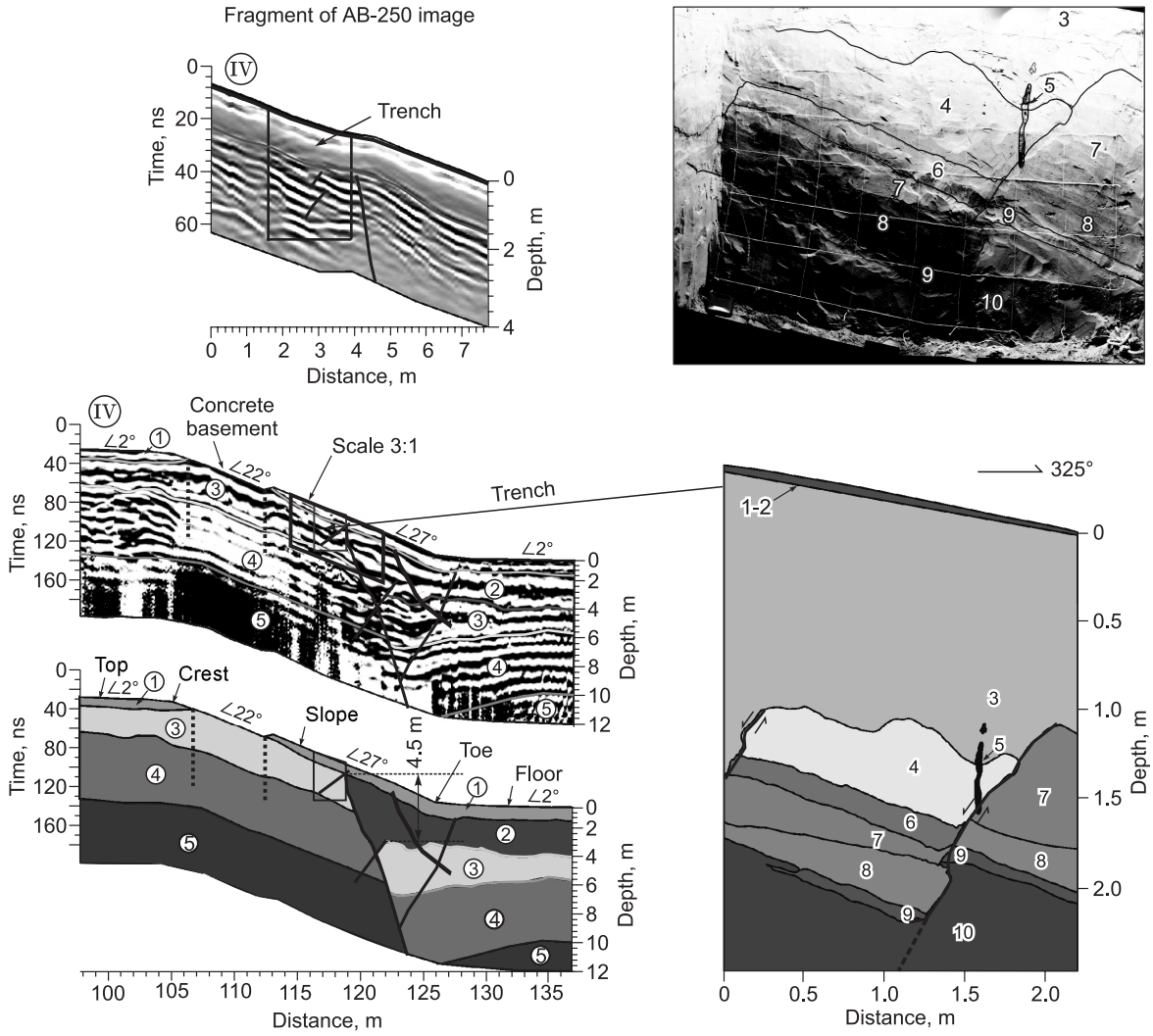

Fig. 5. Fragments of radar images along profile IV across the Delta Fault and their interpretation (between Sherashevo and Inkino villages). Top panel: Fragment of AB-250 image; Right top panel: Trench along profile IV. Arabic numerals show lithologies: 1, top soil; 2, dense gray sandy sil; 3, massive yellow-brown fine to medium sand, with plant roots; 4, light brown fine sand with scarce lenses of lumpy humus and plant roots; indistinctly-bedded layers dip concordantly to slope; 5, soil wedge with half-degraded plant remnants; 6, massive brown fine sand; 7, massive fine to silty sand, with scattered mottles of limonitized sand; 8, gray-brown silty sand; 9, indistinctly-bedded reddish fine sand; 10, massive brown sand.

curs in normal faults (McCalpin, 2009). Thus, the currently available knowledge and quite good consistency of offset estimates from structural, GPR, and surface rupture data indicate that gravity sliding contributed considerably into the ground motion during the Tsagan earthquake.

The local geology and structural pattern of the Delta Fault scarp made basis for 3D modeling of the study area using the Micromine software at Irkutsk National Research Polytechnical University.

Model I (Fig. 6, I) corresponds to the time immediately after the Tsagan event which caused 2.6–4.5 m subsidence of the ground surface on the Delta Fault and produced two conjugate ruptures detectable in the radar images.

Model II (Fig. 6, II) shows the present setting: the fault scarp has been denuded and two subsidiary ruptures appeared, possibly, as a result of the M = 6.8 Central Baikal earthquake of 1959. Previous studies of surface rupture produced by that earthquake (Solonenko and Treskov, 1960) revealed multiple gaping fractures accompanied by mud eruptions over 10 km between Oimur and Dulan villages. Therefore, the subsidiary ruptures in the Delta Fault zone may result from the event of 1959. In general, the structure of the Delta Fault in shallow crust agrees with the known law that the hanging wall in normal faults is more strongly deformed than the footwall (Seminsky et al., 2005).

CONCLUSIONS

The reported results from the Delta Fault segment reactivated by the Tsagan earthquake of 1862 between the villages of Sherashevo and Inkino demonstrate high informa-

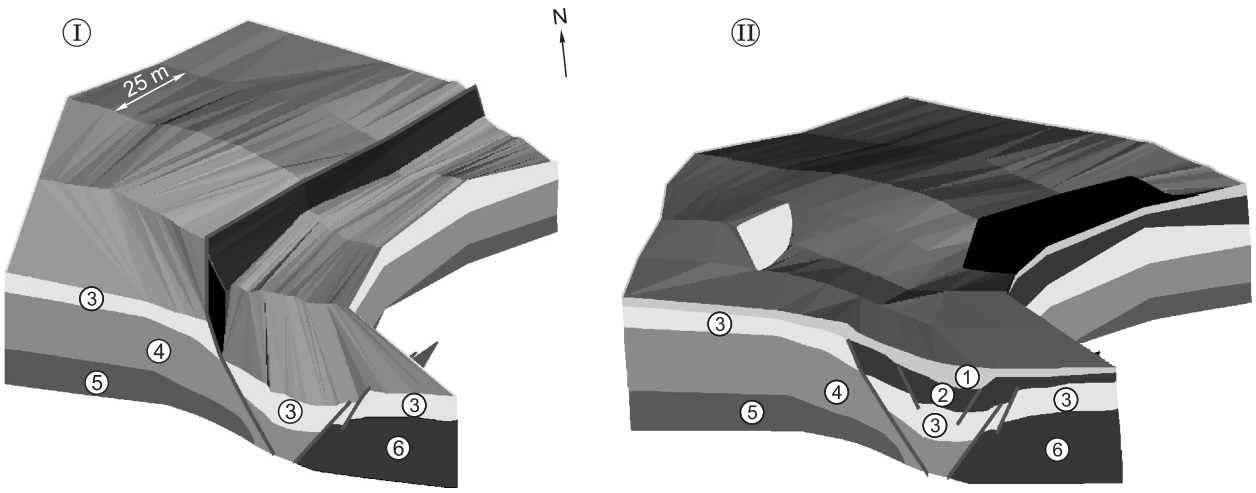

Fig. 6. 3D models of study area. The scarp of Delta Fault in different time periods. Model I: immediately after the earthquake of 1862; model II: at present. 1–6 are GPR units.

tion value of GPR surveys used to image surface rupture in soft sediments. The GPR surveys combined with a small amount of drilling and trenching made it possible to

– trace the main seismogenic rupture over a distance of 100 m and characterize its structure which is common to normal faults;

– estimate the amount of vertical slip on the main seismogenic fault plane, which varies from 2.6 m in the southwest to 4.5 m in the northeast, with an error of ±0.5 m due to the resolution of the AB-90 antenna. The offset estimates generally agree with those measured previously in the trench (Lunina et al., 2012) and on the ground surface right after the earthquake of 1862 (Fitingof, 1865). Therefore, that very event was responsible for the displacement detected and estimated from GPR data;

– estimate the fault plane dip (60–80°) and depth (12 m);

– reveal subsidiary rupture, possibly produced by the M = 6.8 Central Baikal earthquake of 1959;

– distinguish GPR units to the depth 12 m, which correspond to sedimentary layers with different dielectric permittivities;

– model in 3D the fault scarp of the Delta Fault within the study area for different periods of time after the earthquake;

– infer that a considerable part of ground motion during the earthquake occurred as gravity sliding.

Comprehensive understanding of the displacement pattern along the seismogenic fault requires further study extended to other segments of the fault zone.

We appreciate assistance in the filed by A.M. Afonkina, I.A. Potekhina, M.A. Lipina, and D.D. Perevoznikova from the Laboratory of Tectonophysics at the Institute of the Earth's Crust (Irkutsk).

REFERENCES

Brandes, C., Igel, J., Loewer, M., Tanner, D.C., Lang, J., Müller, K., Winsemann, J., 2018. Visualisation and analysis of shear-deformation bands in unconsolidated Pleistocene sand using ground-penetrating radar: Implications for paleoseismological studies. Sediment. Geol. 367, 135–145.

Del'yansky, E.A., 1993. Traces of earthquake-induced soft-sediment deformation in the maximum intensity zone of the Tsagan earthquake, in: Workshop on Geology and Mineral Deposits of East Siberia, Book of Abstracts, Irkutsk, pp. 7–8.

Fisher, T., Štěpančíková, P., Karousova, M., Tábořík, P., Flechig, C., Gaballan, M., 2012. Imaging the Mariánské Lázně Fault (Czech Republic) by 3-D ground-penetrating radar and electric resistivity tomography. Stud. Geophys. Geod. 56, 1019–1036.

Fitingof, A.Kh., 1865. Description of the area at the Selenga Mouth, collapsed by earthquakes of 30 and 31 December 1861. Gornyi Zhurnal 3 (7), 95–101.

Khromovskikh, V.S., 1995. Seismic-induced deformation of crust at and around epicenters of large earthquakes, in: Logachev, N.A., Khromovskikh, V.S. (Eds.), Modern Dynamics of Continental Lithosphere [in Russian]. Nedra, Moscow, pp. 440–503.

Kondorskaya, N.V., Shebalin, N.V. (Eds.), 1982. New catalog of strong earthquakes in the USSR from ancient times through 1977. World Data Center A for Solid Earth Geophysics. Colorado, USA.

Lopatin, I.A., 1862. On earthquakes at the Selenga mouth and nearby. Amur, Newspaper of East Siberia, No. 11, 7 February, 1862.

Lunina, O.V., Gladkov, A.S., Orlova, L.A., 2009. Paleoseismicity in cis-Baikal rifts basins: Evidence and age constraints. Dokl. Earth Sci. 427 (5), 751–754.

Lunina, O.V., Andreev, A.V., Gladkov, A.S., 2012. The Tsagan earthquake of 1862 on Lake Baikal revisited: a study of secondary coseismic soft-sediment deformation. Russian Geology and Geophysics (Geologiya i Geofizika) 53 (6), 594–610 (775–796).

Lunina, O.V., Gladkov, A.C., Afonkin, A.M., Serebryakov, E.V., 2016. Deformation style in the damage zone of the Mondy fault: GPR Evidence (Tunka basin, southern East Siberia). Russian Geology and Geophysics (Geologiya i Geofizika) 57 (9), 1269–1282 (1616–1633).

Lunina, O.V., Gladkov, A.S., Gladkov, A.A., Denisenko, I.A., 2018. Srednekedrovaya paleoseismodislocation in the Baikal ridge: its structure and throws estimated from ground-penetrating radar data. Geodinamika i Tektonofizika 59 (2), 531–555.

McCalpin, J.P. (Ed.), 2009. Paleoseismology. Academic Press, Burlington. Vol. 95.

Robert, G.P., Raithatha, B., Sileo, G., Pizzi, A., Pucci, S., Walker, J.F., Wilkinson, M., McCaffrey, K., Phillips, R.J., Michetti, A.M., Guer-

rieri, L., Blumetti, A.M., Vittori, E., Cowie, P., Sammonds, P., Galli, P., Boncio, P., Bristow, C., Walters, R., 2010. Shallow subsurface structure of the 2009 April 6 M_w 6.3 L'Aquila earthquake surface rupture at Paganica, investigated with ground-penetrating radar. Geophys. J. Int. 183, 774–790.

Salvi, S., Cinti, F.R., Colini, L., D'Addezio, G., Doumaz, F., Pettinelli, E., 2003. Investigation of the active Celano-L'Aquila fault system, Abruzzi (central Apennines, Italy) with combined ground-penetrating radar and palaeoseismic trenching. Geophys. J. Int. 155, 805–818.

Seminsky, K.Zh., Gladkov, A.S., Lunina, O.V., Tugarina, M.A., 2005. The Structure of Continental Fault Zones: The Applied Aspect [in Russian]. Izd. SO RAN, Novosibirsk.

Solonenko, V.P., Treskov, A.A., 1960. The Central Baikal Earthquake of 29 August 1959 [in Russian]. Irkutskoe Knizhnoe Izdatelstvo, Irkutsk.

Strom, A.L., Nikonov, A.A., 1997. Relations between the seismogenic fault parameters and earthquake magnitude. Izv. Phys. Sol. Earth, No. 12, 55–67.

Tarabanko, A.V., 2007. GPR for studies of faults associated with earthquakes in the area of the Poperechnaya River (South Kamchatka). Vestn. KRAUNC, Nauki o Zemle, No. 9, 154–158.

Varenkov, V.V., Volkomirskaya, L.B., Dzhamirze, V.A., Karpuzov, A.F., Karpuzov, A.A., Lobzin, V.V., Reznikov, A.E., 2006. Russian georadar technologies in Australia. Razvedka i Okhrana Nedr, No. 6, 45–50.

Vladov, M.L., Starovoitov, A.V., 2004. Fundamentals of Ground Penetrating Radar Surveys [in Russian]. Moscow University Press, Moscow.

Yalciner, C.C., Altunel, E., Bano, M., Meghraoui, M., Karaback, V., Akyuz, H.S., 2013. Application of GPR to normal faults in the Büyük Menderes Graben, Western Turkey. Geodynamics 65, 218–277.

Editorial responsibility: I.S. Novikov